Lock-in Demodulation of Pulsed Ultrasonic Signals in High Noise Environments

Alec Bales-D'Cruze, Andy Adler, and Carlos Rossa
Department of Systems and Computer Engineering, Carleton University, Ottawa, Canada.
alecbalesdcruze@cmail.carleton.ca; adler@sce.carleton.ca; carlos.rossa@carleton.ca

***Abstract*—Acoustoelectric tomography (AET) maps tissue conductivity by locally modulating its electrical impedance with an ultrasonic wave in the presence of an electric field. The resulting nanoVolt-level, periodic pulsed signals are often buried in extreme noise levels, making traditional filtering and demodulation methods ineffective. This paper examines the feasibility and limitations of using lock-in demodulation to detect these signals in environments with low signal-to-noise ratios (SNR). While lock-in demodulation is traditionally designed to operate on continuous sinusoidal waveforms, its application and effectiveness to demodulate short and exponentially decaying pulsed signals has not been previously investigated.**

The paper presents a discrete model of a lock-in demodulation scheme and verifies it experimentally with ultrasound pulses measured in a phantom tissue and fed to a commercially available lock-in amplifier. The model is then used in a series of simulations to investigate the influence of model and signal parameters, such as filter order, cut-off frequency, pulse width, and SNR, on the demodulation scheme's output. The results indicate that wider wavelets and higher-order filters with a narrow band allow for better noise rejection. The results can guide the design and use of lock-in demodulation schemes for pulsed ultrasonic signals and ultimately offer a more robust alternative to traditional demodulation methods used in AET.

I. Introduction

Acoustoelectric tomography (AET) is an emerging imaging technique that uses focused ultrasound to locally modulate the conductivity of tissue exposed to an electric field while measurements of the electric potential are taken at different locations, enabling high-resolution mapping of the tissue's electrical properties [1]. It is based on the principle that a focused ultrasonic wave travelling through the medium induces microscopic periods of compression and rarefaction at a frequency that corresponds to that of the ultrasonic wave. These changes in volume are spatially encoded at the focal point and alter the tissue's conductivity within, proportionally to the tissue's acoustoelectric coupling constant [1], [2], [3].

When an electric current is applied to tissue in the presence of the acoustic pressure, the induced voltage exhibits low- and high-frequency components. The low-frequency component matches the frequency of the applied current and corresponds to the voltage observed in the absence of pressure. The high-frequency component matches that of the ultrasonic wave and arises from the acoustic modulation of the tissue conductivity. Separated from filtering, the latter provides sufficient information to infer the electrical impedance of the focal point. When the focal point is steered across the tissue, the conductivity can be estimated at any desired point, allowing for high-resolution mapping of the tissue's electrical properties. A major challenge in AET is to extract the weak (nV) high-frequency signal from the dominant carrier frequency buried in background noise. This weak signal-to-noise ratio (SNR) requires accurate filtering and signal processing to reliably isolate and interpret the high-frequency component needed for conductivity mapping.

Traditional narrow-band filters with an amplification stage are generally ill-suited for demodulating such weak periodic signals. While they can be tuned to filter out a frequency of interest, they often introduce significant signal distortion and delay, limiting the time-domain resolution of the transients present in ultrasonic pulses. Furthermore, they are highly sensitive to background noise, often resulting in unstable and unpredictable performance in dynamic environments [4].

Other measurement schemes can be implemented using analog circuits or digital signal processing (DSP). Analog demodulation typically obtains the signal's phase and magnitude through in-phase and quadrature methods [5] at a specific frequency. To detect signals at a different band, the system needs to be replicated, increasing complexity and hardware requirements. In contrast, DSP samples the signal at a constant rate and performs demodulation digitally [5] with either integer-period demodulation and non-integer-period demodulation methods. In the former, the required number of samples is obtained over one or more multiples of the carrier period, resulting in precise and undistorted measurement of the signal's amplitude and phase, but with limited demodulation speed. Non-integer-period demodulation involves sampling over a non-integer number of the carrier period, which can introduce errors, loss of accuracy, and spectral artifacts due to incomplete cycles and signal truncation, offering a trade-off between speed and accuracy [5].

Rectification is one of the simplest forms of integer demodulation. It takes the absolute value of the waveform before low-passing it to extract the signal's envelope or amplitude [6]. While effective for single-frequency demodulation, it is susceptible to multiple frequency components, offering minimal rejection of signals away from the carrier. A more robust approach, the switching method, first multiplies the signal by a reference square wave at the carrier frequency. The low-pass filter then averages out all components that

This research is supported by the Ontario Graduate Scholarship and the Ontario Ministry of Colleges and Universities Early Researcher Award.

do not match the carrier to zero, leaving only the DC term produced when the carrier is multiplied by the square wave, thereby extracting the original signal's envelope [7]. However, switch timing errors and limited bandwidth can introduce phase errors, incomplete sampling, and feed-through noise, which is more pronounced in high frequencies, such as the range used in AET. Another method, called synchronous sampling, limits such timing errors and incomplete sampling by precisely aligning sampling to an integer multiple of the carrier frequency [8]. However, it relies on precise control of the carrier frequency and sampling clock, making it prone to frequency drift. Quadrature demodulation methods improve upon these techniques by capturing both the in-phase and quadrature components of the signal, reducing the errors seen in single-channel methods. It is also better suited for signals with varying frequency contents and wide bandwidths [9]. However, when the carrier or modulating frequency is unknown or varies, or when multiple frequencies must be analyzed concurrently, the discrete Fourier transform (DFT) is a more suitable alternative. It maps the time-domain signal into its frequency components, providing an accurate estimate of the magnitude of each frequency within the signal of interest [10], [11]. Yet, this technique can suffer from spectral leakage when the signal does not contain an integer number of periods within the sampling window, resulting in a widened frequency spectrum and reduced accuracy [12]. It also lacks the time resolution required for tracking spatially localized changes present in AET signals.

An alternative to the above demodulation methods for applications with extremely low SNR is lock-in amplification, a frequency-dependent narrow-band filter capable of detection and measurement of extremely small AC signals buried in noise. This scheme multiples the input signal with a reference sinusoidal signal that matches the frequency of the signal of interest, and then passes the result through a low-pass filter, isolating a DC output proportional to the amplitude of the modulated signal and the reference signal [13]. This approach rests on the principle of orthogonality of sinusoidal functions: when two sine waves of different frequencies are multiplied and integrated over a complete period (or low-passed), the result is zero. The output of the filter is only non-zero if a portion of the signal of interest matches the frequency of the reference signal. This makes lock-in demodulation exceptionally sensitive even in extremely noisy environments.

While a lock-in amplifier can effectively demodulate a *continuous* sinusoidal signal with an exceptional SNR of interest, AET uses instead short-pulsed ultrasound waves that decay exponentially over a temporal length typically not exceeding a couple of microseconds. Therefore, a low-pass filter with a typical time constant designed for optimal noise rejection can distort the resulting pulse envelope and suppress fast signal changes, potentially degrading both the accuracy and timing precision needed for effective demodulation in AET [14]. This paper investigates the feasibility and limits of using lock-in amplification to recover such short-pulsed signals rather than continuous sinusoids. To that end, we devise a model of a lock-in demodulation scheme and verify it with experimental results. The model is then used in a series of simulations to investigate the influence of filter and signal parameters in the amplifier's output. The results can guide the design and use of lock-in demodulation schemes in AET and ultimately offer a more robust alternative to traditional demodulation methods. While lock-in amplification has been proven as an effective solution in low SNR environments for continuous sinusoidal signals, its use for short-duration pulsed signals has not been thoroughly studied and represents the contribution of this work.

The goal of this paper is to characterize the performance of a lock-in amplifier to demodulate pulsed signals, and it is organized as follows. Section II models pulsed ultrasonic signals using wavelets and presents a complete deviation of the lock-in demodulation scheme. The model is subsequently validated experimentally in Section III using ultrasonic signals measured in a phantom tissue and a commercial lock-in amplifier. Once the model is validated, it is used in Section IV to extrapolate the results to a wider range of experimental scenarios to study how the model parameters influence the output of the demodulation scheme.

II. Lock-in Demodulation of Pulsed Signals

A lock-in amplifier multiplies a sinusoidal signal measured in the presence of noise by a reference signal of the same frequency. The result is low-pass filtered, removing any high-frequency components, and leaving a DC signal whose magnitude is proportional to that of the measured sinusoidal signal. Take, for example, the case of the two multiplied cosine waves of frequencies ω_1 and ω_2 and magnitudes A_1 and A_2:

$$\begin{aligned} V(t) &= A_1 \sin(\omega_1 t) A_2 \sin(\omega_2 t) \\ &= \frac{A_1 A_2}{2} [\cos([\omega_1 - \omega_2]t) - \cos([\omega_1 + \omega_2]t)]. \end{aligned} \quad (1)$$

where t is time. When $\omega_1 = \omega_2$, the above simplifies to:

$$V(t) = \frac{A_1 A_2}{2} [1 - \cos(2\omega_1 t)] \quad (2)$$

The result is a signal with both a DC component and one at $2\omega_1$, i.e., at twice the reference frequency. When the signal is low-pass filtered to remove the $2\omega_1$ component and any higher frequency noise, the result is $A_1 A_2/2$, that is, proportional to the magnitude of the signal of interest. In the following subsection, we detail and extend this model to accept a pulsed ultrasonic signal as the input.

A. Modelling an Ultrasonic Pulse

An ultrasonic pulse may be modelled as a sinusoidal carrier wave whose amplitude is modulated by an exponentially decaying envelope. It can be approximated by the Morlet wavelet as:

$$y(t) = A_u e^{-\frac{t^2}{2\sigma^2}} \cos(\omega_u t) \quad (3)$$

where ω_u is the central (ultrasonic) frequency, $A_u = y(0)$ is the peak magnitude of the pulse, and σ is the standard deviation of its Gaussian envelope. The temporal width t_w

of $y(t)$ where its magnitude is greater than mA_u, with $0 < m < 1$ representing the fraction or percentage of A_u, is found by equating the Gaussian envelope to $A_u m$ and solving for $t = t_w$:

$$A_u e^{-\frac{t_w^2}{2\sigma^2}} = A_0 m \rightarrow t_w = \sigma\sqrt{2\ln(m)}. \tag{4}$$

To construct a periodic signal of these pulses with a repetition period of T, we sum time-shifted versions of (3) as

$$Y(t) = \sum_n y(t - nT) = A_u \sum_n e^{-\frac{(t-nT)^2}{2\sigma^2}} \cos\left(\omega_u[t - nT]\right) \tag{5}$$

where $n \in \mathbb{Z}$ is the number of pulses. Further, we assume that $Y(t)$ is observed in the presence of background noise, which is modelled as a sum of sinusoidal components with higher frequencies than the carrier frequency ω_u as

$$\psi(t) = Y(t) + \sum_j A_j \cos\left(\omega_j t + \varphi_j\right) \tag{6}$$

where A_j is the amplitude, ω_j is the angular frequency, and φ_j is the phase of the j^{th} frequency component, with $\omega_u < \omega_j$ assumed for simplicity.

The objective of the lock-in demodulation is to extract the envelope magnitude of the pulse train $Y(t)$ from the observed mixed signal $\psi(t)$, even when the magnitude of the background noise is several orders of magnitude greater than the peak magnitude A_u of $y(t)$.

B. Lock-in Demodulation

In lock-in demodulation, the measured signal $\psi(t)$ is first multiplied by a reference sinusoidal waveform $\cos(\omega_r t)$ of frequency ω_r. When the frequency of the reference waveform matches the centre frequency of the ultrasonic signal, i.e., $\omega_r = \omega_\psi$, the resulting signal produces a DC component proportional to the magnitude of the carrier, and another component at twice the frequency. A low-pass filter then removes the high-frequency component, leaving only the time-dependent DC term that approximates the envelope of the carrier.

The mixing product $\Psi(t) = \psi(t)\cos(\omega_r t)$, is

$$\Psi(t) = \left[Y(t) + \sum_n A_j \cos\left(\omega_j t + \varphi_j\right)\right] \cos(\omega_r t) \tag{7}$$

Replacing (5) in the above and expanding the multiplication using the identity for the product of cosines gives:

$$\begin{aligned}\Psi(t) =& \frac{A_u}{2} \sum_n e^{-\frac{(t-nT)^2}{2\sigma^2}} \Big\{ \cos\left[(\omega_u - \omega_r)t - \omega_u nT\right] \\ &+ \cos\left[(\omega_u + \omega_r)t - \omega_u nT\right] \Big\} \\ &+ \frac{1}{2} \sum_j A_j \Big\{ \cos\left[(\omega_j - \omega_r)t + \varphi_j\right] \\ &+ \cos\left[(\omega_j + \omega_r)t + \varphi_j\right] \Big\}.\end{aligned} \tag{8}$$

For $\omega_r = \omega_u$, the above simplifies to:

$$\begin{aligned}\Psi(t) =& \frac{A_u}{2} \sum_n e^{-\frac{(t-nT)^2}{2\sigma^2}} \left[\cos(\omega_r nT) + \cos(2\omega_r t - \omega_r nT)\right] \\ &+ \frac{1}{2} \sum_j A_j \Big\{ \cos\left[(\omega_j - \omega_r)t + \varphi_j\right] \\ &+ \cos\left[(\omega_j + \omega_r)t + \varphi_j\right] \Big\}.\end{aligned} \tag{9}$$

To simplify the notation, the higher frequency terms will be encompassed by the term $\phi(t)$ such that

$$\Psi(t) = \frac{A_u}{2} \sum_n e^{-\frac{(t-nT)^2}{2\sigma^2}} \cos(\omega_r nT) + \Phi(t). \tag{10}$$

where

$$\begin{aligned}\Phi(t) =& \frac{A_u}{2} \sum_n e^{-\frac{(t-nT)^2}{2\sigma^2}} \cos(2\omega_r t - \omega_r nT) \\ &+ \frac{1}{2} \sum_j A_j \Big\{ \cos\left[(\omega_j - \omega_r)t + \varphi_j\right] \\ &+ \cos\left[(\omega_j + \omega_r)t + \varphi_j\right] \Big\}\end{aligned} \tag{11}$$

The next step is to pass $\Psi(t)$ through a low-pass filter. If the filter's cut-off frequency ω_c satisfies $\omega_c \ll \omega_r$ and $\omega_c < |\omega_j - \omega_r|$, all higher frequency terms are attenuated to near zero ($\Phi(t) \rightarrow 0$), and the only remaining term is

$$\Psi_f(t) \approx \frac{A_u}{2} \sum_n e^{-\frac{(t-nT)^2}{2\sigma^2}} \cos(\omega_r nT). \tag{12}$$

The above approximation indicates that the output of lock-in amplification is proportional to the envelope of the input ultrasonic pulse. This is easily observable when $n = 0$. However, this approximation neglects the time delay and gain introduced by the low-pass filter in the output response. In AET, such pulses occur on the microsecond scale, and accurate timing is crucial for image reconstruction. Therefore, the actual time-domain response of $\Psi_f(t)$ must be calculated.

C. Low-Pass Filtering

A typical implementation of a low-pass filter in a lock-in amplifier takes the form of the following transfer function

$$\frac{\Psi_f(s)}{\Psi(s)} = \frac{1}{\left(\frac{s}{\omega_c} + 1\right)^q} \tag{13}$$

where s is the Laplace variable, and $q \in \mathrm{Z}^*$ is the filter order.

For a first-order filter, $\Psi_f(t)$ can be calculated as the solution of the following differential equation, which is the inverse Laplace transform of (13) when $q = 1$, as:

$$\frac{1}{\omega_c}\frac{d\Psi_f(t)}{dt} + \Psi_f(t) = \Psi(t). \tag{14}$$

When substituting (10) into the above, the resulting equation becomes nonhomogeneous and does not have a closed-form solution. A discretized solution can instead be found by letting

$$t_k = t_0 + k\Delta t, \quad k = 0, 1, \ldots, N,$$

where t_0 is the initial time, assumed to be zero for simplicity, Δt is the sampling time step, and t_k is the discrete time step. Eq. (14) can be approximated as:

$$\frac{\Psi_f(t_{k+1}) - \Psi_f(t_k)}{\Delta t} = \omega_c \left[\Psi(t_k) - \Psi_f(t_k)\right], \tag{15}$$

or simply:

$$\Psi_f(t_{k+1}) = \Psi_f(t_k)(1 - \omega_c \Delta t) + \Psi(t_k)\omega_c \Delta t \tag{16}$$

from which we obtain the filtered signal as:

$$\begin{aligned}\Psi_f(t_{k+1}) =& \Psi_f(t_k)(1 - \omega_c \Delta t) \\ &+ \left[\frac{A_u}{2} \sum_n e^{-\frac{(t_k - nT)^2}{2\sigma^2}} \cos(\omega_r nT) + \Phi(t_k)\right] \omega_c \Delta t.\end{aligned} \tag{17}$$

If a second-order filter is used instead, the filter's output is the temporal solution of (13) for $q = 2$, satisfying:

$$\frac{d^2\Psi_f(t)}{dt^2} + 2\omega_c \frac{d\Psi_f(t)}{dt} + \omega_c^2 \Psi_f(t) = \omega_c^2 \Psi(t). \tag{18}$$

In its discrete form, the solution of the above can be found as

$$\begin{aligned}\frac{\Psi_f(t_{k+1}) - 2\Psi_f(t_k) + \Psi_f(t_{k-1})}{\Delta t^2} + 2\omega_c \frac{\Psi_f(t_k) - \Psi_f(t_{k-1})}{\Delta t} \\ + \omega_c^2 \Psi_f(t_k) = \omega_c^2 \Psi(t_k),\end{aligned}$$

which can be rearranged as

$$\begin{aligned}\Psi_f(t_{k+1}) =& \left(2 - 2\Delta t \omega_c - \omega_c^2 \Delta t^2\right) \Psi_f(t_k) \\ &+ \left(2\Delta t \omega_c - 1\right) \Psi_f(t_{k-1}) + \omega_c^2 \Delta t^2 \Psi(t_k)\end{aligned} \tag{19}$$

to give the filter's output $\Psi_f(t)$ in the form of

$$\begin{aligned}\Psi_f(t_{k+1}) =& \left(2 - 2\Delta t \omega_c - \omega_c^2 \Delta t^2\right) \Psi_f(t_k) \\ &+ \left(2\Delta t \omega_c - 1\right) \Psi_f(t_{k-1}) \\ &+ \left[\frac{A_u}{2} \sum_n e^{-\frac{(t_k - nT)^2}{2\sigma^2}} \cos(\omega_r nT) + \Phi(t)\right] \omega_c^2 \Delta t^2.\end{aligned} \tag{20}$$

The process to find the filtered signal $\Psi_f(s)$ for higher-order filters ($q > 2$) follows the sample steps and will therefore be omitted for simplicity.

Note that when the measured signal is multiplied by the reference cosine in (7), we assume the reference signal $\cos(\omega_r t)$ and the cosine component of the ultrasonic centre frequency $\cos(\omega_u t)$ are in phase. To compensate for any phase shift, we use quadrature demodulation by first mixing the measured signal $\psi(t)$ with a second reference signal shifted by 90°:

$$\Psi_\pi(t) = \psi(t) \cos\left(\omega_r t + \frac{\pi}{2}\right) \tag{21}$$

The process from (7) to the filtering step is repeated for this quadrature component. If the filtered version of $\Psi_\pi(t)$ is $\Psi_{\pi f}(t)$, we retrieve the magnitude of the phase-shifted signal by combining the in-phase and quadrature components as:

$$\Psi_s(t) = \sqrt{\Psi_f(t)^2 + \Psi_{\pi f}(t)^2}. \tag{22}$$

Having defined the output of the lock-in demodulation scheme, we must now define metrics to quantify the quality of the output signal and evaluate the influence of the lock-in amplifier's tunable parameters on the output.

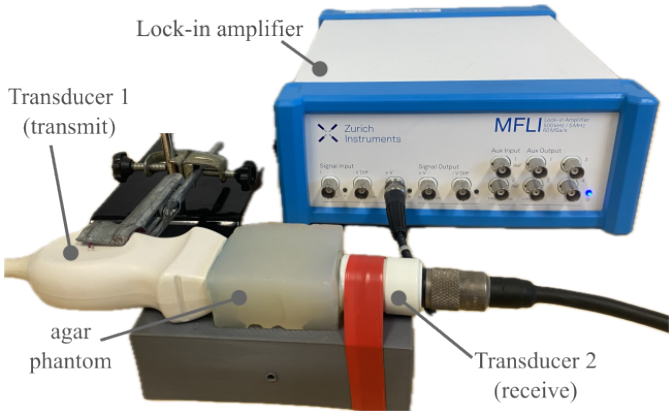

Fig. 1: Experimental setup for model validation. Transducer 1 emits a pulsed ultrasound waveform through an agar phantom at a repetition frequency of 30Hz and centre frequency of 2.25 MHz. The waveform measured by transducer 2 is input into the lock-in amplifier.

D. Output Signal Quantification

The input wavelet function has three main parameters: amplitude A_u, pulse width σ, and frequency ω_u. By varying these parameters, a family of different wavelets can be generated and tested. To these wavelets, we add variable amounts of noise by simulating $\Phi(t)$ in (11) as additive white Gaussian noise, thereby creating input signals with different SNRs.

The tunable parameters of the lock-in amplifier are its filter's cut-off frequency ω_c and order q.

To evaluate the influence of these parameters in the demodulation of the pulsed signal, the following metrics are defined to quantify the quality of the output signal $\Psi_f(t)$ in comparison to the reference input $\psi(t)$:

1) The amplitude of the demodulated signal;
2) The time delay τ elapsed between the peak of the output signal with respect to the peak of the input wavelet;
3) The SNR of the output signal.

III. Experimental Model Validation

To validate the proposed model, we use the experimental setup shown in Fig. 1. A 128-element phased array transducer (P4-1 from Philips Healthcare, Andover, MA, USA), placed in contact with a gel phantom made of 4% agar and distilled water, is driven at 2.25 MHz by an ultrasound system (Vantage LE 64 from Verasonics, Kirkland, WA, USA). The probe emits single pulses of ultrasound waves roughly 10 μs in duration, at a repetition rate of 30 Hz. On the opposite side of the phantom, we place a single-element transducer to measure the resulting waveform. The single-element transducer is directly connected to the input of a 5 MHz lock-in amplifier (MLFI from Zurich Instruments, Zurich, Switzerland). The distance between the two transducers is 60 mm.

The lock-in amplifier's reference frequency is set to $\omega_r = 2.25$ MHz with a third-order filter and a -3 dB cutoff frequency of $\omega_c = 241$ kHz. The signal measured by the

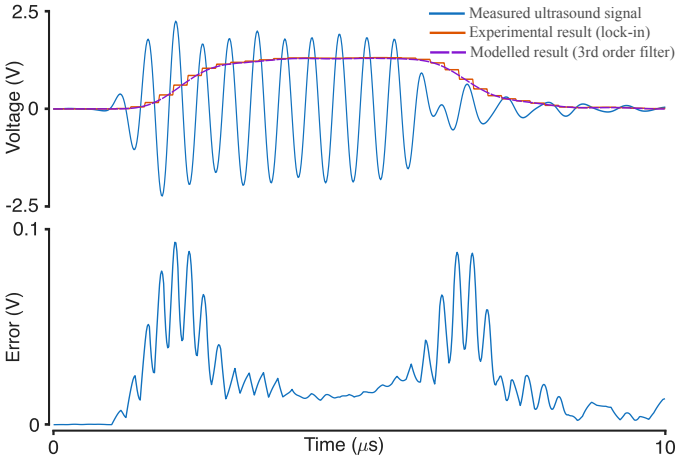

Fig. 2: Measured single ultrasonic pulse (blue), experimentally demodulated signal (orange), and model-estimated demodulated signal (dashed purple) using a third-order filter (top panel). The bottom panel shows the absolute error between the model and the lock-in amplifier's output.

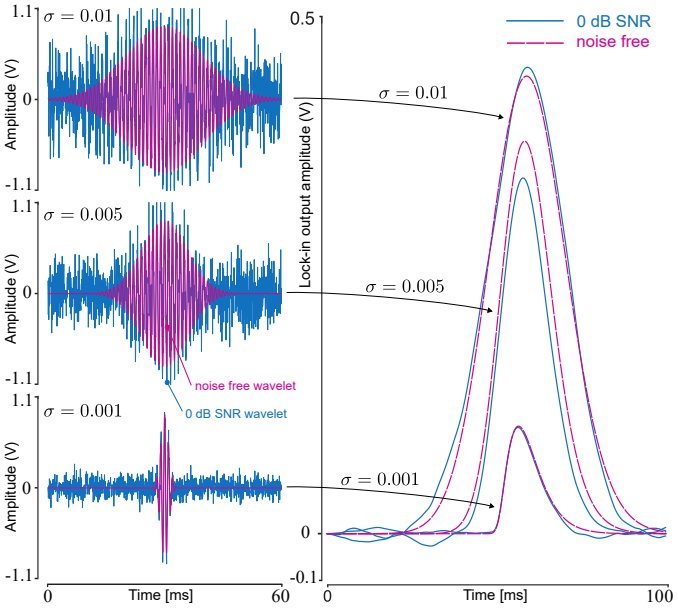

Fig. 3: Effect of wavelet width (Gaussian envelope σ) on the output signal for wavelets with no noise (purple) and with a 0 dB added SNR (blue). The input wavelets in the left 3 panels have a frequency of 1 kHz. The corresponding lock-in amplifier output on the right is calculated with a third-order filter with a cut-off frequency of 50 Hz.

single-element transducer is processed in the lock-in amplifier and also input into the model described earlier, which is tuned with the same parameters as the lock-in amplifier.

Fig. (2) shows the raw ultrasonic pulse detected by the receiving transducer along with the demodulated signals calculated by the lock-in amplifier and through the proposed model. The results show an overlap of the experimental and modelled signals. Noting that the lock-in amplifier introduces a 1 μs time delay due to internal processing, these signals are time-shifted in the plot by the same amount. The spikes in the error plot are a result of the discretization of the output signal and the sampling resolution of the lock-in amplifier.

Having validated the accuracy of the proposed model, the model can now be used to extrapolate the experimental conditions to different combinations of input signals and demodulation parameters.

IV. Simulation Results

First, we evaluate the influence of the duration of the wavelet pulse (i.e., the Gaussian envelope width σ) on the lock-in amplifier's output. The left side of Fig. 3 shows 3 wavelets simulated with a centre frequency of $\omega_u = 1$ kHz and different Gaussian envelopes $\sigma = 0.01$, $\sigma = 0.005$, and $\sigma = 0.001$, resulting in different pulse widths and numbers of cycles. The purple line represents the noise-free wavelet, while the blue signals have an added white Gaussian noise. The right side of the figure shows the respective demodulated lock-in-demodulated output for a third-order filter and a cut-off frequency of 50 Hz. The results indicate that the magnitude of the output increases with the wavelet width, and wider wavelets offer better noise rejection.

Next, we evaluate the influence of the cut-off frequency and the filter order in the amplifier's output. The input wavelet is simulated with a centre frequency of 1 kHz and a Gaussian envelope of $\sigma = 0.001$. Fig. 4 (a) shows the time elapsed between the peak of the input wavelet and the peak of the demodulated signal for different filter orders as a function of the cut-off frequency, while Fig. 4 (b) shows the resulting peak magnitude of the output signal. These results indicate that: 1) the higher the filter order, the higher the time delay, 2) the higher the filter order, the lower the peak magnitude of the output signal, and 3) the lower the cut-off frequency, the higher the time delay and the lower the peak magnitude for a given filter order. In Fig. 4(c), we added three different levels of noise to the input signal (10 dB, 0 dB, and -10 dB SNR) and evaluated the resulting SNR of the output. The results show that more aggressive filters improve the SNR of the output, at the cost of lower peak magnitude and higher time delay. A lower-order filter with a larger bandwidth has the least time delay, yet it may include spurious frequencies.

Finally, we evaluate the influence of the Gaussian envelope σ on the output SNR for 3 different input SNRs using the same wavelet and filter parameters described earlier. Fig. 5 shows that wider wavelets increase the output SNR. This is because wider wavelets allow the low-pass filter to average the signal over a longer time window with more frequency components, improving rejection of broadband noise components are do not match the reference frequency.

V. Conclusion

In this paper, we model and evaluate the performance of a lock-in amplifier in demodulating pulsed signals across various experimental and simulation conditions. The model

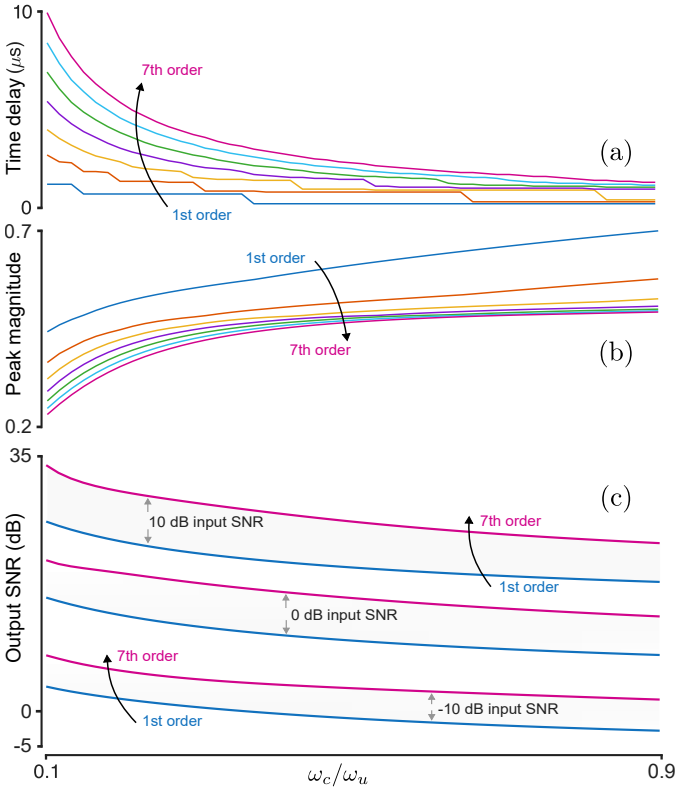

Fig. 4: Influence of cut-off frequency ω_c relative to the wavelet centre frequency ω_c and filter order on: 1) the time delay between the input and output peak magnitude (a), 2) the peak magnitude of the output signal (b), and 3) the SNR of the output (c). Each of the three grey zones in the bottom panel indicates a different input SNR.

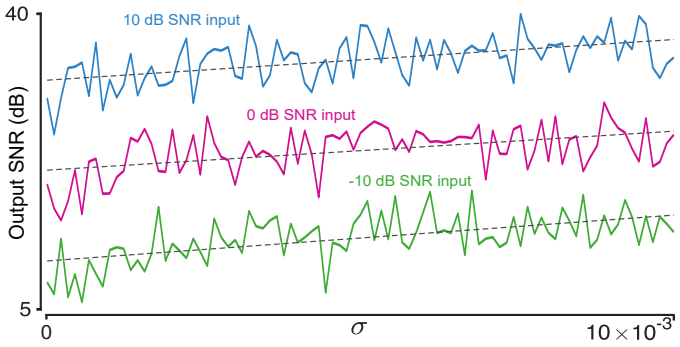

Fig. 5: Effect of wavelet width (Gaussian envelope σ) on the output SNR for wavelets with 3 different SNR as the model input. The lock-in amplifier output assumes a third-order filter with a cut-off frequency of 50 Hz.

is first verified experimentally with pulsed ultrasound signals measured in a phantom tissue, and then used to extrapolate the operating conditions in simulations using a wider range of model and input wavelet parameters to determine optimal parameters for signal demodulation.

The results show that:

- Wider wavelets allow more effective noise averaging, resulting in higher output magnitude and better noise rejection;
- Higher order filters and low cut-off frequencies increase time delay and reduce output magnitude, but improve output SNR;
- Output SNR improves for all tested input SNRs as the wavelet width increases and the cut-off frequency decreases.

While the input signal must have sufficient frequency components to be detected, the filter parameters must strike a balance between order and bandwidth to capture the signal without letting unwanted noise through while minimizing time delay. These findings can guide the development of efficient experimental setups to measure the acoustoelectric effect in challenging experimental conditions.

References

[1] B. Keeshan, A. Adler, and C. Rossa, "Improved configurations for 3d acoustoelectric tomography with a minimal number of electrodes," *IEEE Transactions on Biomedical Engineering*, vol. 70, no. 12, pp. 3501–3512, 2023.

[2] C. McDermott, H. A. Bidgoli, and C. Rossa, "Observation of the ultrasonic vibration potential with an instrumented coaxial needle probe," in *2023 IEEE International Instrumentation and Measurement Technology Conference (I2MTC)*. IEEE, 2023, pp. 1–6.

[3] B. Keeshan, A. Adler, and C. Rossa, "Reduced effective sensitivity of acoustoelectric tomography," *International Journal of Bioelectromagnetism*, vol. 24, 2022.

[4] S. Sun, L. Xu, Z. Cao, W. Yang *et al.*, "Signal demodulation methods for electrical tomography: A review," *IEEE Sensors Journal*, vol. 19, no. 20, pp. 9026–9035, 2019.

[5] S. Sun, L. Xu, Z. Cao, j. sun, and W. Yang, "Signal demodulation methods for electrical tomography: A review," vol. 19, no. 20, pp. 9026–9035. [Online]. Available: https://ieeexplore.ieee.org/abstract/document/8746631

[6] S. Sun, L. Xu, Z. Cao, H. Zhou, and W. Yang, "A high-speed electrical impedance measurement circuit based on information-filtering demodulation," *Measurement Science and Technology*, vol. 25, no. 7, p. 075010, 2014.

[7] L. Xu, H. Zhou, Z. Cao, and W. Yang, "A digital switching demodulator for electrical capacitance tomography," *IEEE Transactions on Instrumentation and Measurement*, vol. 62, no. 5, pp. 1025–1033, 2013.

[8] M. Min, T. Parve, A. Ronk, P. Annus, and T. Paavle, "Synchronous sampling and demodulation in an instrument for multifrequency bioimpedance measurement," *IEEE Transactions on instrumentation and Measurement*, vol. 56, no. 4, pp. 1365–1372, 2007.

[9] N. Daldal, M. Nour, and K. Polat, "A novel demodulation structure for quadrate modulation signals using the segmentary neural network modelling," *Applied Acoustics*, vol. 164, p. 107251, 2020.

[10] Z. Wang, P. Ingram, R. Olafsson, C. L. Greenlee, R. A. Norwood, and R. S. Witte, "Simulation-based optimization of the acoustoelectric hydrophone for mapping an ultrasound beam," in *Medical Imaging 2010: Ultrasonic Imaging, Tomography, and Therapy*, vol. 7629. SPIE, 2010, pp. 249–260.

[11] C. Candan, M. A. Kutay, and H. M. Ozaktas, "The discrete fractional fourier transform," *IEEE Transactions on signal processing*, vol. 48, no. 5, pp. 1329–1337, 2000.

[12] D. A. Lyon, "The discrete fourier transform, part 4: spectral leakage," *Journal of object technology*, vol. 8, no. 7, 2009.

[13] J. H. Scofield, "Frequency-domain description of a lock-in amplifier," *American journal of physics*, vol. 62, no. 2, pp. 129–132, 1994.

[14] L. Zhu, J. Wu, G. Lin, L. Hu, and H. Li, "Improving the signal-to-noise ratio in ultrasound-modulated optical tomography by a lock-in amplifier," in *Optics in Health Care and Biomedical Optics VII*, vol. 10024. SPIE, 2016, pp. 690–696.